INJURY BIOMECHANICS RESEARCH
Proceedings of the Thirty-Ninth International Workshop

Development of the Global Human Body Models Consortium Mid-Sized Male Full Body Model

F. Scott Gayzik[1,2], Daniel P. Moreno[1,2], Nicholas A. Vavalle[1,2],
Ashley C. Rhyne[1,2], Joel D. Stitzel[1,2]

[1]Virginia Tech – Wake Forest University Center for Injury Biomechanics
[2]Wake Forest University School of Medicine, Department of Biomedical Engineering

ABSTRACT

This study describes the development and validation of a full human body finite element model created for use in crash injury biomechanics research as part of the Global Human Body Models Consortium (GHBMC) project. The geometry of the model is based on a protocol that leverages the strengths of three clinical scanning methods; computed tomography (CT), magnetic resonance imaging (MRI), and upright MRI (i.e. subject in seated position). The protocol was applied to a living male volunteer (26 years, height, 174.9 cm, and weight, 78.6 kg) who met extensive anthropometric and health criteria. Computer Aided Design (CAD) data were developed from the images, containing significant anatomical detail. A region-specific development approach was used, with five Body Region Centers of Expertise (COEs) focused on meshing and validation of the Head, Neck, Thorax, Abdomen, and Plex (Pelvis and Lower Extremity). The regional models were then integrated into a full body model. Mesh connections between neighboring body regions were assembled using techniques based on the geometry, element type, and anatomic purpose. This consisted of nodal connections for all 1-D beam and discrete element connections (e.g. ligamentous structures), 2D shells (e.g. the inferior vena cava to right atrium), and many 3D tetrahedral and hexahedral structures (e.g. soft tissue envelope connections between body regions). In cases where node-to-node connections were not made, (e.g. 3D muscle to bone insertions), contact definitions were implemented. The integrated full body model consists of 1.3 million nodes, and 1.9 million elements. Element types in the model are 41.0 % hexahedral, 33.8 % tetrahedral, 19.5 % quad shell, 5.1% tri shell, and 0.6 % others including beam and discrete elements. Non-linear and/or viscoelastic material models were used where appropriate. Simulations were conducted using LS-DYNA MPP971 R.4.2.1. The model has been validated against a number of frontal and lateral rigid impactor and sled tests. Two of these validation cases are highlighted in this work, displaying the model kinematics and kinetics. Through the use of a living subject, comprehensive image data, and extensive geometric validation, this model has the potential to provide a greater degree of accuracy in blunt trauma simulations than existing human body models. It will serve as the foundation of a global effort to develop a family of next-generation computational human body models for injury prediction and prevention.

INTRODUCTION

There are an estimated 1.2 million automotive-related deaths worldwide each year with more than 50 million non-fatal injuries (WHO 2009). Motor vehicle crashes are the leading cause of death for people ages 5 to 34 in the United States (CDC 2007). Computational human body models validated in blunt injury are a potentially powerful new tool to study injury mechanisms which can lead to improved safety designs for vehicles. Computational models have been used in the field for more than 50 years (Yang 2006). The focus of this study is a seated full human body finite element model developed as part of the Global Human Body Models Consortium (GHBMC) project. The development and validation results for two cases are presented.

Currently there are two models commercially available for use in injury biomechanics research – the Total Human Model for Safety (THUMS) (Toyota 2010; Iwamoto, Kisanuki, et al. 2002) and the Human Model for Safety (HUMOS) (Robin 2001). The THUMS model has increased in complexity with each successive release and the current version has about 1.8 million elements. THUMS includes geometry from supine CT images of an individual that was a close match to the 50th percentile male. The model contains a significant amount of anatomical detail (Shigeta, Kitagawa, et al. 2009). The current version of HUMOS has approximately 102,000 elements (Bidal 2008). The HUMOS model geometry is from sections of a cadaver frozen in the seated driver occupant position. The mesh of HUMOS can be scaled in a range from the 5th percentile female to the 95th percentile male (Serre 2006). Unlike previous research, the geometry of the model presented here was generated from a multi-modality imaging protocol collected in a prospective manner for the expressed purpose of finite element model development.

The GHBMC is an international consortium of automakers and suppliers working with research institutes and government agencies to advance human body modeling for crash simulations. The goal of the consortium is to concentrate human body modeling research efforts into a single global effort. Ultimately, a set of human body models will be developed and validated based on the work of the consortium. Wake Forest University is the Integration Center of Expertise (COE) in the consortium. The role of the Integration COE in Phase I of this effort was to recruit subjects to serve as templates for model generation, to acquire medical images and anthropometry of the subjects, to develop computer aided design (CAD) data from the medical images, to assemble body region models (BRMs) into a single full body model (FBM) and to perform validation simulations on the full body model. This paper focuses on the development of the 50th percentile male (M50) FBM from subject recruitment through model validation results. There are nearly 20 simulations in which the model has been tested; a small subset of those will be presented here.

The GHBMC M50 FBM is intended for use in vehicle crash simulations and is positioned as a seated driver occupant. The model was developed in LS-DYNA 971 R4.2.1 (LSTC, Livermore, CA). A regional modeling approach was used wherein models of the Head, Neck, Thorax, Abdomen, and Plex (Pelvis and Lower Extremity) were developed independently and integrated into a single FBM. The model has been developed to simulate kinematic and kinetic responses of the body in the blunt injury loading regime.

METHODS

Medical Imaging and CAD Development

Detailed descriptions of the CAD development and external anthropometry can be found in the literature (Gayzik 2012; Gayzik 2011). For completeness these will be briefly reviewed. The subject recruited to represent the M50 model was 26 years old, 78.6 kg, 174.9 cm, and in excellent health. The subject matched within 5% of fifteen anthropometric targets from a survey by the U.S. Army (Gordon, Churchill, et al. 1989). Imaging data were collected using supine Magnetic Resonance Imaging (MRI), upright MRI, and Computed Tomography (CT). External anthropometry and bony landmarks were collected in the undeformed seated posture using a custom buck and a three-dimensional digitizer (FARO Technologies Inc., Lake Mary, FL). The image collection protocol was approved by the Wake Forest University School of Medicine Institutional Review Board (IRB). Supine MRI data were collected on a 1.5 Tesla Twin Speed scanner (GE, Milwaukee, WI). A three-dimensional Fast Spoiled Gradient Recalled pulse sequence was used to facilitate segmentation of the data into various structures. These data were used to obtain soft tissue anatomy. The upright MRI data were collected on a 0.6 Tesla Fonar Upright MRI (Fonar Inc., Melville, NY). Upright MRI was used to capture bone and soft tissue shapes and locations oriented in a seated posture with gravitational effects. Three-dimensional gradient echo pulse sequences similar to MRI were used for this modality. CT scans were acquired using a GE LightSpeed, 16-slice scanner, software revision 07MW11.10, service pack 2 (GE, Waukesha, WI). Images were acquired in helical model with the subject in the supine and an approximately seated position. Imaging modalities can be seen in Figure 1.

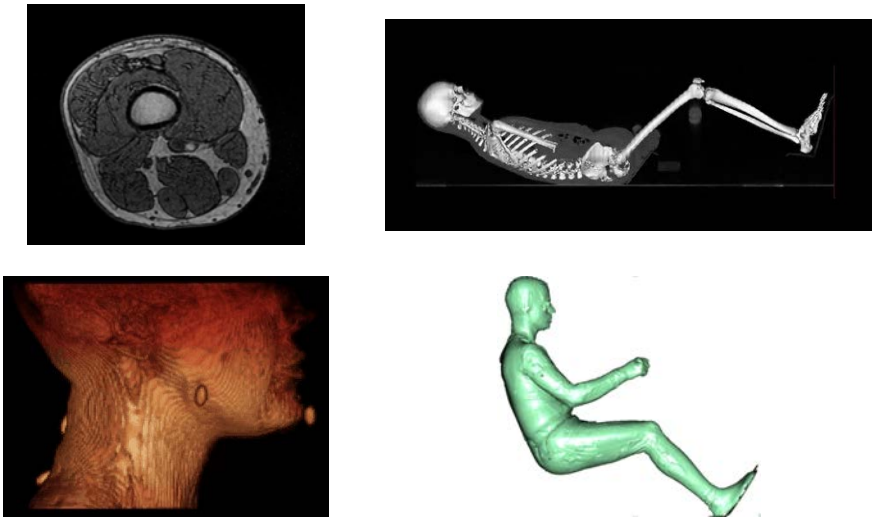

Figure 1. Overview of data collected for full body CAD development. Clockwise from upper left, conventional MRI thigh cross section, quasi-seated CT scan, external body laser scan in seat buck (raw point data), and upright MRI, lateral view of neck

CAD data of these medical images were created using the following process. First, segmentation was performed using one of three means – automatic, semi-automatic, and manual segmentation. Automatic segmentation was used only where atlas-based algorithms were available, predominantly in white and gray matter of the brain. A semi-automated approach was used primarily in segmenting bone where a threshold could be used since contrast between the structure and surrounding area was large. Manual segmentation had to be used in most other soft tissues. The segmentations were conditioned to match upright MRI organ locations and morphologies. Non-Uniform Rational Basis-Spline (NURBS) surfaces were developed on the conditioned polygon data. Border continuity was enforced so that neighboring patches were tangentially continuous. Sagittal symmetry was induced where appropriate. The final CAD dataset included 418 parts, with 179 individual bones described by 216 parts, 46 organs and components, 96 muscles, 37 blood vessels, and 26 ligaments, tendons and cartilaginous structures, seen in Figure 2. The CAD data was developed primarily from the medical images of the recruited subject; however, the anatomy was also rigorously checked against the literature (Gayzik 2011).

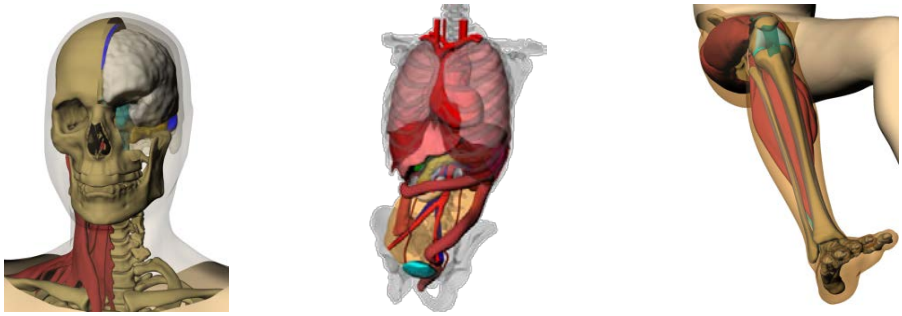

Figure 2. CAD data of M50, Left to right, detail of head and neck, detail of thorax and abdomen, detail of lower extremity.

Model Integration

CAD data were split into five regions and five Body Region Models (BRMs) finite element models were developed by partner research institutes in the GHBMC. The BRMs were developed and validated by the following regional breakdown, as seen in Figure 3 – Head, Neck (DeWit 2012; Fice 2011), Thorax (Li 2010; Li 2010), Abdomen (Beillas 2012), and Plex (Yue 2011). The regional models were delivered to the Integration COE for assembly into the M50 FBM. Each of the four interface integration strategies will be briefly reviewed below; further details can be found in the literature (Thompson 2012). Model integration was performed using LS-PrePost (v. 3.1 LSTC, Livermore, CA) and HyperMesh (v. 11, Altair Inc., Troy, MI).

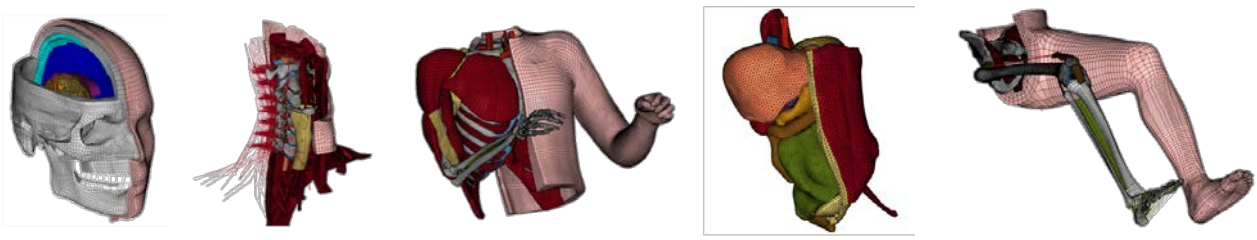

Figure 3. Body Region Models (BRMs). Left to Right, Head, Wayne State University (PI's K. Yang and L. Zhang), Neck, The University of Waterloo (PI, Duane Cronin), Thorax, University of Virginia (PI's R. Kent and D. Subit), Abdomen, IFSTTAR & Virginia Tech (PI's Philippe Beillas and Warren Hardy) and Plex, The University of Virginia (Pelvis and Lower Extremity COE, PI's Costin Untaroiu, Jeff Crandall and Alan Eberhardt of the University of Alabama-Birmingham).

Head-Neck Interface. The cartilage on the skull was remeshed due to penetrating elements with C1. The hyoid bone, modeled as a rigid body, was attached to the skull using discrete 1D elements. The 52 volumetric muscles that were modeled in the neck were attached to the skull and cervical spine via tied contacts. Ligaments, fibers, and all 1D elements (36 muscles and 8 ligament groups) were connected to the head model via nodal connections. Head and neck flesh models were also connected with node to node continuity. Remeshing was conducted to complete the connection between the brainstem and spinal cord. The head-neck interface is seen in Figure 4.

Figure 4. Head-Neck model integration example. Left, lateral view of deep structures, Right, posterior view of neck muscles tied to skull.

Neck-Thorax Interface. All 1D neck muscles (n=62), 1D neck ligaments (n=4), and 3D neck muscles (n=52) were attached to the appropriate thoracic bony landmarks. Tied contacts were used for 3D muscles (Figure 5) while nodal connections were made for all 1D elements. The superior facet of T1 was modified for node to node agreement with the neck model. The thorax and neck flesh components were connected via shared nodes. Ligamentous connections, modeled as 1D elements, from the neck model along the cervical spine were connected to T1.

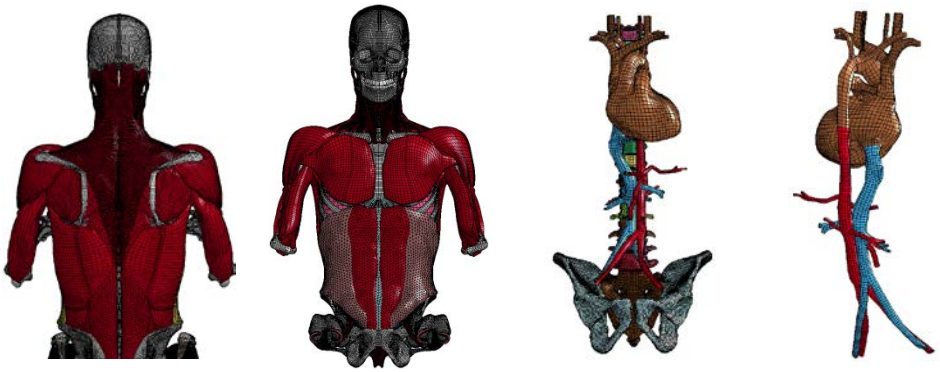

Figure 5. Neck-Thorax and Thorax-Abdomen model integration examples. Left to right: posterior view of back musculature, anterior view, anterior view of heart and great vessels, posterior view.

Thorax-Abdomen Interface. Tied contacts were used between thoracic anatomy and abdominal muscles (Figure 5). Abdominal 1D ligaments were connected to the diaphragm via nodal connections. The thoracic and

abdominal portions of the great vessels were connected via shared nodes. Superior lumbar kinematic constraints were verified. The thoracic and lumbar vertebrae are modeled as rigid bodies.

Abdomen-Pelvis Interface. Tied contacts from the thoracic and abdominal muscles to the pelvis and lower extremity bony landmarks were made (Figure 5 and Figure 6). The lumbar spine was integrated to the sacrum using a rigid plate. The plate was created from a set of nodes on the superior sacrum (Figure 6) and constrains L5-S1 kinematic joint beam nodes since the sacrum is modeled as deformable and the lumbar spine vertebrae are modeled as rigid bodies.

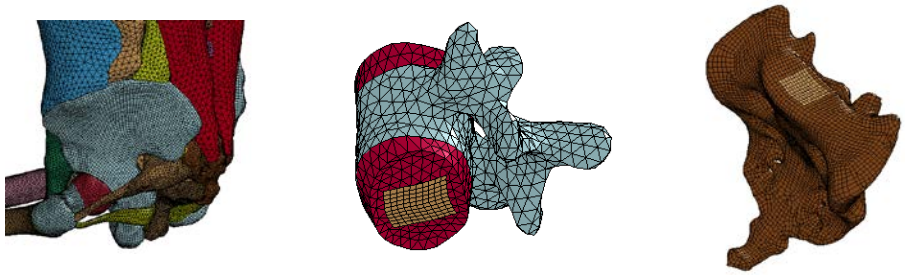

Figure 6. Abdomen- Plex Model integration. Right, muscles with tied contacts. Middle, left, plate used to constraint the lumbar spine to the sacrum.

The Integration COE was responsible for modeling the soft tissue flesh around the entire full body model. The current version of the model uses a simplified rubber model (Mat 181 in LS-Dyna). The tension response is based on tensile loading of the Sartorius muscle in the literature (Yamada 1970) and the compression response is based on a simulated block compression test using material parameters from the literature (Untaroiu, Darvish, et al. 2005). The current version of the model contains 1.96 million elements, 847 parts, and weighs 75.1 kg.

Validation

There have been almost 20 impact scenarios, both frontal and lateral, in which the M50 model has been tested. Two of these will be presented in this current work – a lateral thoracoabdominal impact (Viano 1989) and a passenger frontal sled test (Forman, Lessley, et al. 2006). These two simulations were chosen for this overview since they present both the kinetics (thoracoabdominal impact) and the kinematics (sled simulation) of the model. The thoracoabdominal impact used a 23 kg cylindrical impactor striking an area 7.5 cm below the xiphoid process at a 60° lateral rotation from the anterior. The impact simulated occurred at a nominal velocity of 6.7 m/s. The subjects (n=9) in this experimental study were suspended upright with their arms overhead. The passenger sled tests were performed using a force-limiting passenger belt at 8.1 m/s (n=3). The subject's hands in this setup were allowed to rest on the lap. Repositioning of the model was not performed in either case; all simulations were run in the seated driver position. Simulations were run using LS-Dyna MPP971 R4.2.1 on a Linux Red Hat computational cluster maintained at Wake Forest University (DEAC Cluster). In this study force traces, peak force, and number of rib fractures were compared to the experimental results of the thoracoabdominal impact. Number of fractures, chestband contour at maximum deflection, and phototarget trajectories of the head, shoulder, hip, and knee were compared in the sled case.

RESULTS

M50 Full Body Model Integration

Summary statistics of the M50 model are found in Table 1. The mass distribution by region is found in Figure 7 and a picture of the integrated model can be found in Figure 8. The largest region by both element count and mass is the Plex region comprising roughly 50% of the mass and a third of the elements (Figure 7 and Figure 9). The Neck model contains roughly 260 x 10^3 elements due to modeling each neck muscle with solid hexahedral elements (Figure 4, Figure 5, Figure 8, and Figure 9). Element types used in the model are summarized in Figure 10. The most common element type found in the model is solid hexahedral, comprising 41% of the model. The M50 brain, thorax, and lower extremity are majority hexahedral elements. Many soft tissue structures within the abdomen are modeled with solid tetrahedral elements. Solid tetrahedral elements are the second most common element type found in the model, comprising 33.8% of all elements.

Table 1. FBM 3 Model Summary statistics

Number of Elements / Nodes	1.95 x 106 / 1.30 x 106
Number of Parts	847
Number of Materials	557
LS-DYNA build used to test model for validation	R 4.2.1 Rev.: 53450 Prod. ID: 54013
MPP on high performance cluster computer	mpp971_s_R4.2.1_Intel_linux86-64_hpmpi
Model Mass (kg)	75

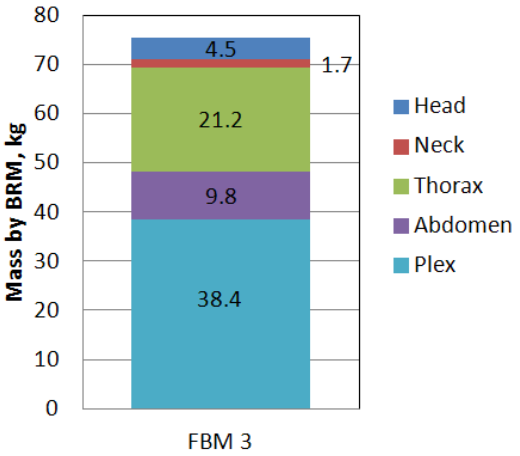

Figure 7. Model mass distribution by BRM showing the total mass for each region.

Figure 8. Oblique view of the M50 model, seated, with half the flesh layer elements not visible, to show underlying structures.

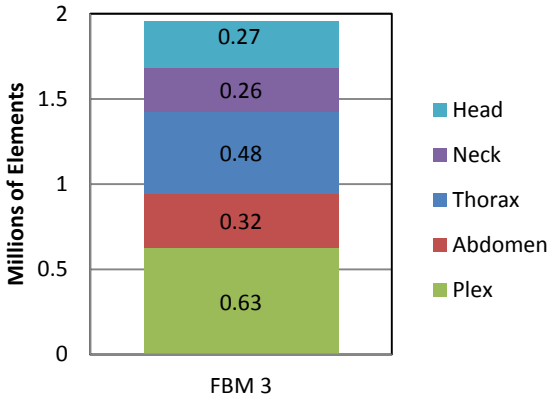

Figure 9. Element breakdown by BRM within the FBM model.

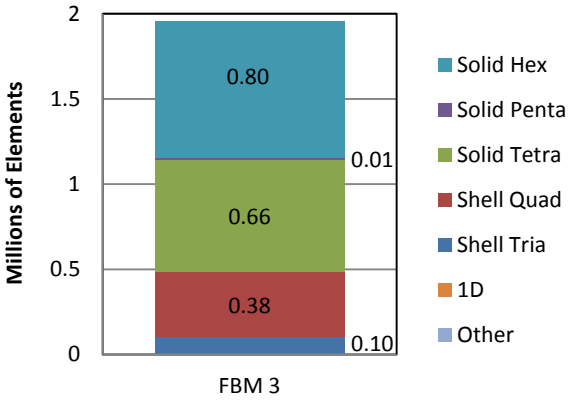

Figure 10. Element breakdown by element type within the FBM model.

Hard target element quality standards were set for the Jacobian and tetrahedral collapse criterion. The goal for these "hard targets" was to have 100% adherence to the standards. The standards were: Jacobian greater than 0.4 for shells (quadrilateral and tria) and greater than 0.3 for solid hex elements. Tetrahedral collapse was to be held greater than 0.2. Broadly, all regions met this goal, with noncompliance below 0.005% in all regions. Additional element quality specifications were applied, with a maximum non-compliance of 1% for all regions.

M50 Full Body Model Detailed Description

The M50 model contains detailed anatomy in each body region which we briefly summarize here, first reviewing bone data, then soft tissue data. Layers of the skull bone are modeled individually with hex elements, including the diploë. The neck model contains all relevant bony anatomy including cervical vertebral bodies and the hyoid bone. Long bones in the upper extremity of the model including the humerus, radius, ulna and clavicle are modeled with hexahedral elements for trabecular bone and shell elements for cortical bone. Long bones in lower extremity of the model employ solid hexahedral elements for cortical bone in the midshaft, while the cortical bone in the epiphyseal ends of these bones is modeled with shell elements. Trabecular bone in these cases is modeled with hexahedral elements. The pelvis is modeled with solid hexahedral cortical bones and solid tetrahedral elements for trabecular bone. Ribs are modeled with shell elements for cortical bone and solid hexahedral for cancellous bone. Rib thickness varies regionally. Fracture of the ribs is modeled through the use of piecewise linear plasticity with failure (Li 2010).

The head model contains 17 sub structures of the brain including the white and gray matter, CSF, sinuses, cerebellum, basal ganglia, corpus callosum and ventricles. The tentorium, falx, pia and dura are modeled with shell elements. Neck ligaments are modeled as one-dimensional elements with progressive failure. Facet joints, the annulus fibrosus and nucleus pulposus are also included in the model. The 52 muscles of the neck region are also modeled as three-dimensional hexahedral structures with one-dimensional elements within them. Thorax model contains the heart, lungs, diaphragm and great vessels. Fat pads are used as void filling structures. A number of thoracic muscles relevant to blunt loading are also included such as the pectoralis major, deltoid, biceps, and triceps. The abdomen model contains all major soft tissue organs and vessels including the liver, spleen, kidneys, colon, small bowel, bladder, inferior vena cava, portal vein, descending aorta, and relevant vascular tethers to organs. Muscles of the abdomen including the rectus abdominis, obliques, erector spinae, and quadratus lumborum are modeled as 3-dimensional structures. In the Plex region, muscles of the pelvic rim including the psoas, iliac, piriformis, obturator internus and levator ani are modeled. Within the lower extremity, the knee ligaments including the MCL, LCL, PCL, ACL, menisci, quadriceps tendon and patellar tendon are modeled.

Thus, a large number of distinct anatomical structures were modeled explicitly rather than homogenizing the body's anatomy. A consequence of this approach is that the model contains void space since not all structures could be modeled. However, this void space accounts for only 4.2% of the total model volume. More than half of the total void is found in the thorax, abdomen, and pelvis. Because the mass distribution is extremely important to the kinematics of the model, the location of body segment centers of gravity were thoroughly documented and compared against previous studies, showing good agreement. (Thompson, Rhyne, et al.) The origin of the global coordinate system for the FBM model is located at the H-point of the seat buck. This location corresponds to the central pelvis of the model. A world coordinate system, defined per the SAE J1733 sign convention, was aligned to the mid-sagittal plane. The positive x-direction points anteriorly, the positive y-direction points to the model's right, and the positive z-direction points inferiorly to make a right-handed coordinate system. The model is pre-programmed with a number of output node sets such as head, shoulder, hip and knee photo-targets for tracking kinematics.

Validation

The results from the validation simulations are shown below in Figure 11, Figure 12, and Figure 13. Figure 11 shows time sequences of these two impacts on the M50 model with transparent flesh to show the loading on the underlying structures.

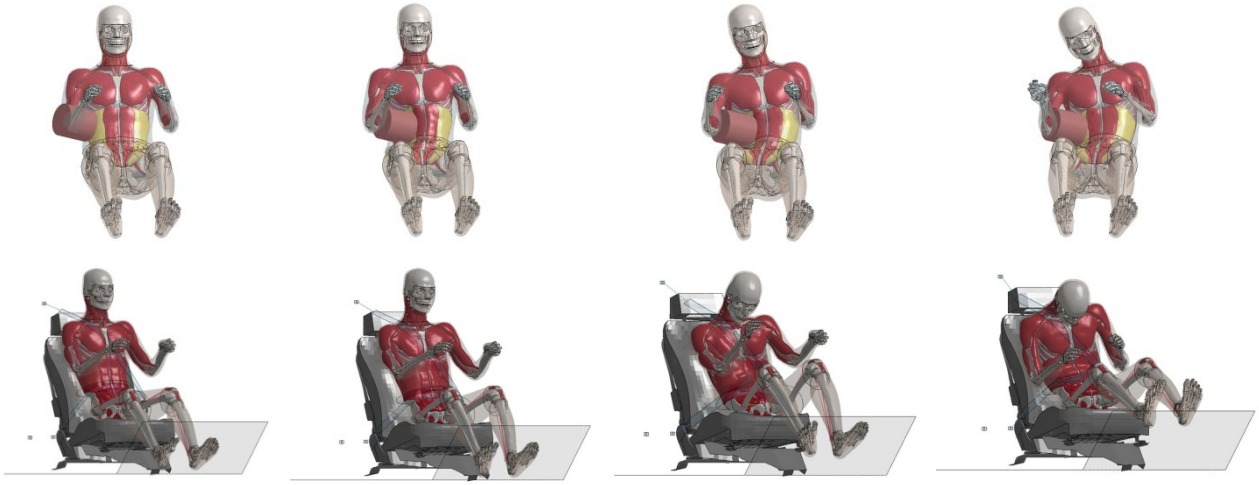

Figure 11. Time lapse sequence of model simulations, thoracoabdominal impact (upper) and passenger sled test (lower).

The impactor force vs. time and force vs. displacement in the thoracoabdominal case can be seen compared to experimental corridors in Figure 12. The model output force trace is just above the corridor in both instances. However, this is just for 12 ms, or 7 cm of displacement, of the simulation while the rest is within the corridors. The model output for peak force is within the corridor in the thoracoabdominal case, and was 4.5 kN while the peak force found experimentally was 4.0±0.26 kN. Four rib fractures, one each in ribs 6-9, were predicted in the model while the experimental tests found a range of 0-7 fractures occurring in ribs 6-10.

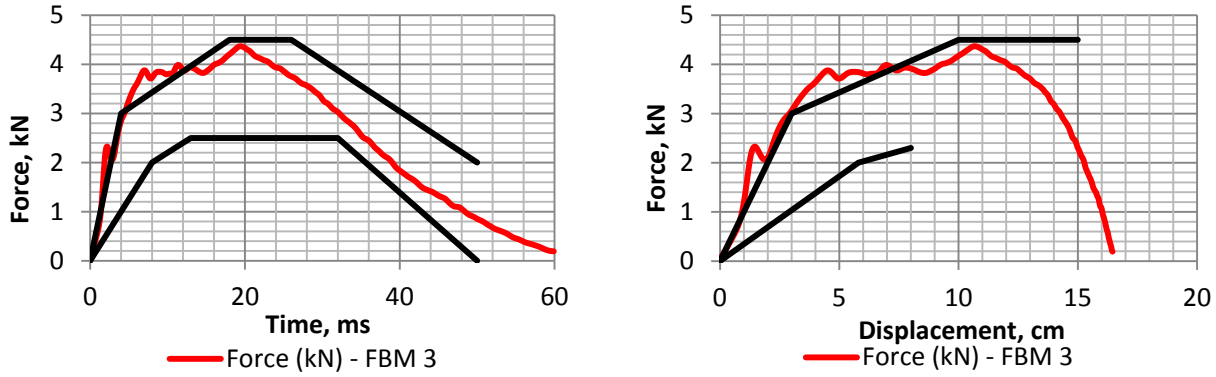

Figure 12. Force vs. time (left) and force vs. displacement (right) in the thoracoabdominal case.

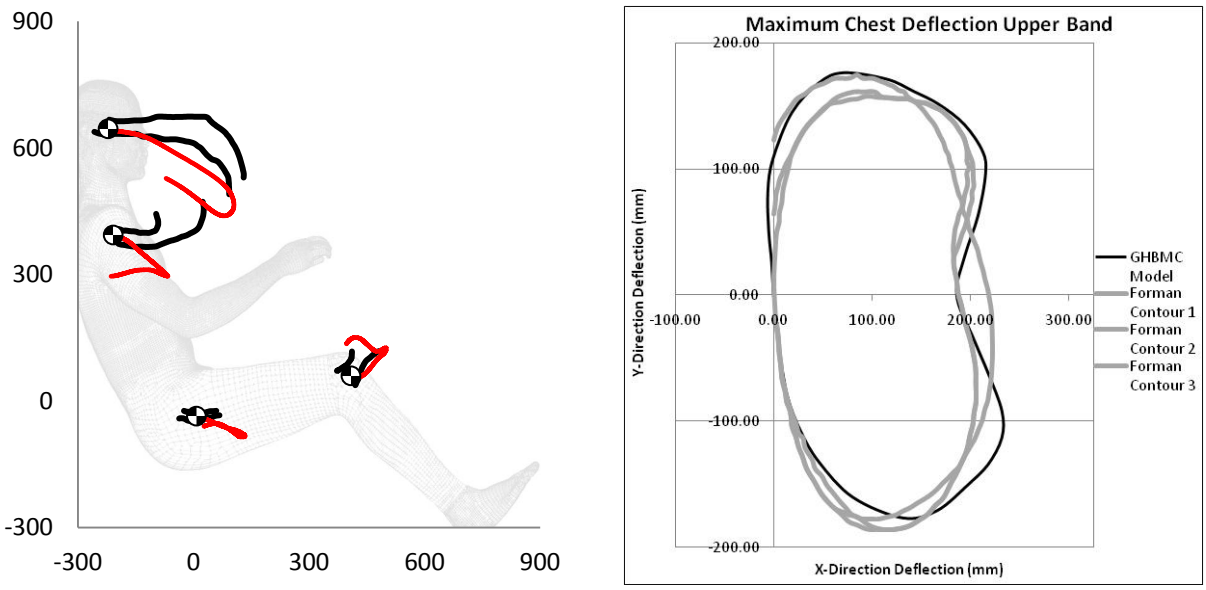

Figure 13. Phototarget trajectory (left, displacements in mm) and chest band comparison (right) in the sled case.

The phototarget trajectories and chestband comparison for the sled case can be seen in Figure 13. Head and knee trajectories followed similar paths to the corridors but were slightly outside the bounds. The shoulder and hip trajectories seemingly followed different paths than what was found experimentally. It should be noted that the seat cushion material used in these tests was a generic seat material that will be more closely matched to the experimental conditions if possible in future work. The chestband contour output from the model compares favorably with 2 of the 3 experimental subjects. While no fractures were predicted in the experimental tests, one fracture in each of ribs 7-9 were predicted in the model.

DISCUSSION

The integration of five regional finite element models into a full body model was presented. In addition, two validation cases that separately highlight the kinematics and kinetics of the model were investigated. The integration of neighboring regions involved many common finite element modeling methods to create a single model. These included nodal connections, 1D discrete elements, tied contacts, and surface to surface contacts. The model validation results showed relatively good agreement in these two cases. In the thoracoabdominal impact the force vs. displacement model output was only slightly outside the corridors for the first 7 cm of displacement and within the corridors for the rest of the event. Additionally, the peak force was only slightly more than one standard deviation away from the average experimental peak force and within the corridors. In the sled case, the phototarget trajectories of the head and knee followed the corridors well while the shoulder and hip trajectories were more divergent. Chestband comparisons in the sled case showed a good match between the model and 2 of 3 subjects; the third contour did not match the other two. Rib fractures predicted in the thoracoabdominal case were within the range of the experimental results. No rib fractures were reported in the sled experiments, yet the model predicted three rib fractures, this may indicate that the seat belt model may be too stiff.

While using cadaveric data for validating a human body model is the current standard in the field, there are limitations that coincide with using this data. Cadavers have both morphologic and material characteristics that make them unlike the living humans which any FBM ultimately aims to represent. Recall that the GHBMC M50 model was created from the scans of a living subject. It has been well established that many cadavers are older and frailer than an average living human. This is especially true in the ribcage where it has been shown that not only do the material properties change, but so do the cortical thickness, rib angle (Kent 2005), and shape (Gayzik 2008). It has also been shown that the elderly are more susceptible to thoracic injury (Stitzel 2010). In the sled tests, only one subject was close to the age of the model (27 years vs. 26 years, respectively) while the majority of subjects were over 60 years old.

One of the limitations of this study is the positioning of the model compared to the experimental subjects. In the thoracoabdominal impact cadavers were held upright by their wrists rather than being seated. It has been found that the thoracic and abdominal organ locations do not differ greatly between a seated and standing position

(Beillas 2009), so we feel this is a worthy simplification in the thoracoabdominal case. In addition, the main axis of the impact is aligned roughly perpendicularly with the trunk of the body through the center of gravity, and no seat was simulated to restrict the motion of the body during impact, therefore more closely matching the experimental condition. The hands of the cadavers in the sleds tests were allowed to rest on the lap of the subject. Rather than attempting to reposition the model to more accurately capture the starting orientation as found in the experiment, the driver posture was maintained. Future studies will focus more on large scale changes in the initial position, however this considered outside the scope of this study. Additionally, the model was not gravitationally settled into the seat of the sled simulation. It is possible that, in the sled case, the initial positioning of the model could account for some of the differences seen in the shoulder and hip trajectories.

CONCLUSIONS

This work presented the development and two validation cases of the Global Human Body Models Consortium (GHBMC) 50th percentile male (M50) model. A multi-modality imaging approach was used in which medical images of a living subject were acquired to create the model geometry. Collaborating institutes created regional models of the Head, Neck, Thorax, Abdomen, and Plex (Pelvis and Lower extremity) from the CAD data created by the Integration Center (Wake Forest University). The five regional models were integrated into one full body model using a variety of techniques common in finite element modeling. Two validation cases were presented in this work, a lateral thoracoabdominal impact and a passenger frontal sled test. Model outputs compared favorably to experimental results in both kinematics and kinetics in these two cases. The GHBMC M50 model is the first in what will be a family of highly biofidelic computational human body models for crash injury prediction and prevention.

ACKNOWLEDGEMENTS

Data appearing in this document were prepared under the support of the Global Human Body Models Consortium (GHBMC) by the Full Body Model Center of Expertise. Any opinions or recommendations expressed in this document are those of the authors and do not necessarily reflect the views of the GHBMC. The authors gratefully acknowledge the contributions of the Body Region Centers of Excellence (COE) in the GHBMC model development at the regional level. This work was conducted by Wayne State University (Head COE, PI's King Yang and Liying Zhang), The University of Waterloo (Neck COE, PI Duane Cronin), The University of Virginia (Thorax COE, PI's Richard Kent and Damien Subit), IFSTARR & Virginia Tech (Abdomen COE, PI's Philippe Beillas and Warren Hardy) and The University of Virginia (Pelvis and Lower Extremity COE, PI's Costin Untaroiu and Jeff Crandall and Alan Eberhardt at the University of Alabama-Birmingham). Dr. Untaroiu is currently faculty at Virginia Tech. The authors also acknowledge Timothy Miller and David Chin for support with the DEAC Computational cluster.

REFERENCES

CENTER FOR DISEASE CONTROL. (2007). Web-based Injury Statistics Query and Reporting System: Leading Causes of Death Report.

WORLD HEALTH ORGANIZATION. (2009). Global status report on road safety. Geneva, Switzerland.

TOYOTA MOTOR CORPORATION. (2010). Documentation of Total Human Model for Safety (THUMS) AM50 Pedestrian/Occupant Model.

BEILLAS, P., BERTHET, F. (2012). Performance of a 50th percentile abdominal model for impact: effect of size and mass. European Society of Biomechanics Conference.

BEILLAS, P., LAFON, Y., SMITH, F. W. (2009). The effects of posture and subject-to-subject variations on the position, shape and volume of abdominal and thoracic organs. Stapp Car Crash J 53: 127-54.

BIDAL, S. (2008). Improving human model, examples of applications. European HyperWorks Technology Conference. Strasbourg, France.

DEWIT, J.A., CRONIN, D.S. (2012). Cervical spine segment finite element model for traumatic injury prediction. Journal of the Mechanical Behavior of Biomedical Materials 10: 138-150.

FICE, J.B., CRONIN, D.S., PANZER, M.B. (2011). Cervical spine model to predict capsular ligament response in rear impact. Annals of Biomedical Engineering 39: 2152-2162.

FORMAN, J., LESSLEY, D., KENT, R., BOSTROM, O. AND PIPKORN, B. (2006). Whole-body kinematic and dynamic response of restrained PMHS in frontal sled tests. Stapp Car Crash J 50: 299-336.

GAYZIK, F., MORENO, D., DANELSON, K., MCNALLY, C., KLINICH, K., STITZEL, JOEL. (2012). External Landmark, Body Surface, and Volume Data of a Mid-Sized Male in Seated and Standing Postures. Annals of Biomedical Engineering. Epub: 23 March 2012.

GAYZIK, F.S., MORENO, D.M., GEER, C.P., WUERTZER, S.D., MARTIN, R.S., STITZEL, J.D. (2011). Development of a Full Body CAD Dataset for Computational Modeling: A Multi-modality Approach. Annals of Biomedical Engineering 39: 2568-2583.

GAYZIK, F.S., YU, M., DANELSON, K.A., SLICE, D.E., STITZEL, J. D. (2008). Quantification of age-related change of the human rib cage through geometric morphometrics. J. Biomech 41: 1545-54.

GORDON, C., CHURCHILL, T., CLAUSER, C., BRADTMILLER, B., MCCONVILLE, J., TEBBETTS, I. AND WALKER, R. (1989). 1988 Anthropometric Survey of U.S. Army Personnel: Methods and Summary Statistics. Prepared for United States Army Natick Research Development and Engineering Center.

IWAMOTO, M., KISANUKI, Y., WANTANABE, I., FURUSU, K., MIKI, K. AND HASEGAWA, J. (2002). Development of a finite element model of the Total Human Model for Safety (THUMS) and application to injury reconstruction. International Research Council on the Biomechanics of Injury (IRCOBI). Munich, Germany.

KENT, R., LEE, S.H., DARVISH, K., WANG, S., POSTER, C.S., LANGE, A.W., BREDE, C., LANGE, D., MATSUOKA, F. (2005). Structural and material changes in the aging thorax and their role in crash protection for older occupants. Stapp Car Crash J 49: 231-249.

LI, Z., KINDIG, M.W., KERRIGAN, J.R., UNTAROIU, C.D., SUBIT, D., CRANDALL, J.R., KENT, R.W. (2010). Rib fractures under anterior-posterior dynamic loads: Experimental and finite-element study. Journal of Biomechanics 43: 228.234.

LI, Z., KINDIG, M.W., SUBIT, D., KENT, R.W. (2010). Influence of mesh density, cortical thickness and material properties on human rib fracture prediction. Medicine Engineering and Physics 32: 998-1008.

ROBIN, S. (2001). Human Model for Safety – A joint effort towards the development of redefined human-like car-occupant models. 17th International Conference for the Enhanced Safety of Vehicles. Amsterdam.

SERRE, T., BRUNET, C., BRUYERE, K., VERRIEST, J.P., MITTON, D., BERTRAND, S., SKALLI, W. (2006). HUMOS (Human Model for Safety) Geometry: from one specimen to the 5th and 95th percentile. SAE Technical Paper 2006-01-2324

SHIGETA, K., KITAGAWA, Y. AND YASUKI, T. (2009). Development of next generation human FE model capable of organ injury prediction. Enhanced Safety of Vehicles. Stuttgart, Germany.

STITZEL, J.D., KILGO, P.D., WEAVER, A.A., MARTIN, R.S., LOFTIS, K.L., MEREDITH, J.W. (2010). Age Thresholds for Increased Mortality of Predominant Crash Induced Thoracic Injuries. Annu Proc Assoc Adv Automot Med 54: 41-50.

THOMPSON, A.B., GAYZIK, F.S., MORENO, D.P., RHYNE, A.C., VAVALLE, N.A., STITZEL, J.D. . (2012). A paradigm for human body finite element model integration from a set of regional models. Biomedical Sciences Instrumentation 48: In Press.

THOMPSON, A.B., RHYNE, A.C., MORENO, D.P., GAYZIK, F.S. AND STITZEL, J.D. Methods for validation of the mass distribution of a full body finite element model - biomed 2011. Biomed Sci Instrum 47: 100-5.

UNTAROIU, C., DARVISH, K., CRANDALL, J., DENG, B. AND WANG, J.T. (2005). A finite element model of the lower limb for simulating pedestrian impacts. Stapp Car Crash J 49: 157-81.

VIANO, D.C. (1989). Biomechanical Responses and Injuries in Blunt Lateral Impact. Stapp Car Crash J 33:

YAMADA, H. (1970). Strength of Biological Materials. Baltimore: Williams and Wilkins Company.

YANG, K.H., HU, J., WHITE, N. A., KING, A. I., CHOU, C. C., PRASAD, P. (2006). Development of numerical models for injury biomechanics research: a review of 50 years of publications in the Stapp Car Crash Conference. Stapp Car Crash J 50: 429-90.

YUE, N., SHIN, J., UNTAROIU, C.D. (2011). Development and validation of an occupant lower limb Finite element model. SAE Technical Paper 2011-01-1128